Water Clusters on Graphite: Methodology for Quantum Chemical A Priori Prediction of Reaction Rate Constants

S. Xu, S. Irle,* D. G. Musaev,* and M. C. Lin*

Department of Chemistry and Cherry L. Emerson Center for Scientific Computation, Emory University, Atlanta, Georgia 30322

Received: June 15, 2005; In Final Form: August 21, 2005

The properties, interactions, and reactions of cyclic water clusters $(H_2O)_{n=1-5}$ on model systems for a graphite surface have been studied using pure B3LYP, dispersion-augmented density functional tight binding (DFTB-D), and integrated ONIOM(B3LYP:DFTB-D) methods. Coronene $C_{24}H_{12}$ as well as polycircumcoronenes $C_{96}H_{24}$ and $C_{216}H_{36}$ in monolayer, bilayer, and trilayer arrangements were used as model systems to simulate *ABA* bulk graphite. Structures, binding energies, and vibrational frequencies of water clusters on mono- and bilayer graphite models have been calculated, and structural changes and frequency shifts due to the water cluster−graphite interactions are discussed. ONIOM(B3LYP:DFTB-D) with coronene and water in the high level and $C_{96}H_{24}$ in the low level mimics the effect of extended graphite π-conjugation on the water−graphite interaction very reasonably and suggests that water clusters only weakly interact with graphite surfaces, as suggested by the fact that water is an excellent graphite lubricant. We use the ONIOM(B3LYP:DFTB-D) method to predict rate constants for model pathways of water dissociative adsorption on graphite. Quantum chemical molecular dynamics (QM/MD) simulations of water clusters and water addition products on the $C_{96}H_{24}$ graphite model are presented using the DFTB-D method. A three-stage strategy is devised for a priori investigations of high temperature corrosion processes of graphite surfaces due to interaction with water molecules and fragments.

Introduction

Graphite is an important surface material especially because it can withstand high temperature and high pressure conditions due to its chemical inertness. In recent years, the interaction of water with graphite has attracted considerable attention, mainly due to the growing technological importance of carbon nanotubes (CNTs) and nanohorns[1−7] and in the context of water serving as a graphite lubricant.[8,9] A less prominent perspective on the water−graphite system is the fact that water is a universal combustion product, and knowledge about its chemical reactions with carbon-based high temperature surface materials is imperative for the design of more advanced, corrosion-free carbon-based combustion chambers and rocket nozzles. Yet, up to now essentially nothing is known about corrosion of graphite surfaces by water or water fragments under conditions of combustion. The extreme nature of this high temperature/high pressure chemistry far away from conventional textbook chemistry presents enormous problems to gain a better understanding of the corrosion processes both from experimental and from theoretical points of view, and no attempt has been reported in the literature to tackle this topic.

Until now, experimental and theoretical studies have only scratched the surface of the problem by studying the interaction of water clusters with graphite and CNT surfaces. In 1995, Kasemo et al. have investigated for the first time water adsorption on graphite using high resolution electron-energy-loss spectroscopy and temperature-programmed desorption,[10] and adsorption isotherms were reported first by Vartapetyan et al.[11] and more recently for pristine[12,13] and oxidized graphite surfaces.[14] In addition, calorimetric studies were performed to estimate adsorption heats of water on graphite surfaces with varying degrees of surface oxidation.[15,16] Furthermore, numerous classical molecular dynamics (MD) studies[17−23] have been carried out, but no definite agreement has even been reached on the basic question as to whether graphite is hydrophobic[18] or can be lubricated by water as found in experiments.[8,9,23] Werder et al. pointed out that this disagreement in MD studies arises mainly from different water monomer binding energies to the graphite surface, due to different choices of the interaction potential parameters.[22] Using the computationally much more expensive MP2 method, Feller and Jordan recently computed the binding energy of the water monomer with a $C_{96}H_{24}$ dicircumcoronene model for a single graphite layer,[24] and improved potentials for MD simulations have been based on their results, which are actually in agreement with the notion of lubricating water clusters on graphite surfaces.[23] (The series coronene−circumcoronene−dicircumcoronene, etc. constitutes a D_{6h} one-isomer polycircumbenzenoid series of hydrocarbon systems.) The controversy is, however, still not settled, as different quantum chemical levels of theory can predict qualitatively different results: while a nonhybrid DFT study did not find significant attraction between a water and a graphite surface,[25] a very recent B3LYP/6-31G(d) study on the $C_{60}@(H_2O)_{60}$ clathrate-like water cluster showed the water−buckyball interaction to be essential for the stability of the $(H_2O)_{60}$ cage.[26] To make the situation even more complicated, the basis set superposition error (BSSE)[27] inherent to quantum chemical cluster calculations is roughly of the same order of magnitude as the water−graphite interaction itself and very difficult to correct, especially in the case of MP2 energetics.[24,28] Very recently, water reactions with single-walled CNTs have been

* Corresponding authors. E-mail: (S.I.) sirle@emory.edu; (D.G.M.) dmusaev@emory.edu; (M.C.L.) chemmcl@emory.edu.

10.1021/jp053234j CCC: $30.25
Published on Web 10/04/2005

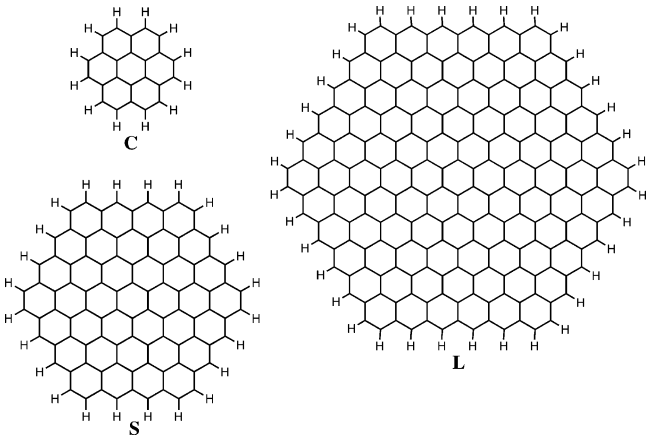

Figure 1. Schematic drawings of coronene $C_{24}H_{12}$ (C) and polycircumcoronenes $C_{96}H_{24}$ (S) and $C_{216}H_{36}$ (L) model systems for graphite layers. Lewis-type π-bond valence structures are omitted.

studied using FTIR spectroscopy and B3LYP/STO-3G calculations on water addition of ideal Stone−Wales tube defects,[7] but no attempt was made to clarify the reaction pathways leading to the C−H and C−OH containing addition products. The same is true for a lower quality HF/Lanl2DZ study[29] on the dissociative adsorption products of water on the coronene $C_{24}H_{12}$ molecule (see Figure 1).

It is our goal to formulate and apply a methodology based on quantum chemical modeling that allows us to accurately and exhaustively investigate reaction pathways for the high temperature dissociative adsorption reaction of water clusters with realistic models for bulk graphite on the best level of quantum molecular theory available and to estimate reaction rate constants that can be used in explaining experimental data on combustion-induced graphite corrosion by water. Clearly, this goal cannot be reached exclusively by making educated guesses for transition states (TSs) and reaction pathways since the energies of the experimental conditions are so high that important regions of the potential energy surfaces (PESs) can be visited, which may not be intuitive to educated TS guesses. As an alternative to traditional reaction pathway guessing, we therefore propose a three-stage methodology for the quantum chemical prediction of reaction rate constants. It is based in stage 1 on a priori reaction pathway identification using unbiased finite-temperature quantum chemical molecular dynamics (QM/MD) simulations, pointing to regions on the PES where important reactant complexes, intermediates, and reaction products can be expected. In stage 2, we will identify these stationary points and their complete reaction pathways quantitatively by performing geometry optimizations from trajectory snapshots at higher levels of theory. In stage 3, we will use the obtained knowledge of the most important reaction conditions and reaction pathway thermodynamics to predict kinetic reaction rate constants for high temperature and high pressure reactions of water with graphite.

In this paper, we present mainly benchmark studies on the reliability of the quantum chemical methods to be employed in the first two stages of our three-stage methodology, using experimental and higher level computational studies on water clusters, models for bulk graphite, and water−graphite complexes, whenever available. Given the complex nature of the problem and the need to perform long canonical molecular dynamics simulations, we are not striving to pinpoint reaction energetic to within fractions of a kcal/mol, but rather, we expect our quantum chemical methods to reproduce experimental structures and spectroscopic data qualitatively correct. Obviously, the underlying potential for QM/MD simulations of stage 1 needs not only to provide reasonable energetics for dissociative water adsorption processes but also to describe the influence of π-conjugation and delicate π-stacking interactions of bulk graphite on these reactions. For this purpose, we are using the density functional tight binding (DFTB) method,[30−32] augmented by a dispersion term,[33] which has been shown to provide computationally inexpensive yet qualitatively accurate descriptions of carbon PESs in high temperature simulations.[34−36] For stage 2 of our methodology, we are using the more accurate ONIOM integrated method[37,38] and combine the ab initio B3LYP[39] level of theory for the high level model system with the dispersion augmented DFTB method for the real system, which is intended to mimic the influence of bulk graphite on the water−graphite surface reactions.

This paper is organized as follows: the next section describes the computational methods employed in more detail. The Results and Discussion contains four subsections: the efficient quantum chemical treatment of bulk graphite, the theoretical description of water−graphite interactions and their influence on water cluster harmonic vibrational frequencies, the identification and characterization of dissociative adsorption pathways of a water molecule on a single graphite layer, and preliminary high temperature QM/MD simulations of water clusters and water dissociation products on a graphite surface. The last section summarizes our findings and presents an outlook on our future work.

Computational Methods

This methodology-oriented work facilitates pure density functional theory (DFT), pure DFTB, and an integrated ONIOM-(DFT:DFTB) approach for quantum chemical electronic structure calculations. In the following paragraphs, we will describe each method employed in greater detail.

The DFTB method,[30,31] as well as its self-consistent-charge (SCC-DFTB) variant,[32] has recently become very popular,[40] largely because of its small computational effort that is roughly equivalent to traditional semiempirical methods while at the same time predicting structures and energetics much more closer to high level DFT. The SCC-DFTB method has been augmented by an empirical Heitler−London type pair-potential term to include dispersion forces (SCC-DFTB-D, we will refer to this method simply as DFTB-D in the remainder of the text), describing for instance the π-stacking in benzo[*a*]pyrene in good agreement with experimental structures.[33] Zhang et al. have recently shown in a comparative study with MP2 that the DFTB-D method is reasonably reliable and efficient in describing small water clusters on a single graphite surface;[41] it is therefore well-suited for the treatment of our large model systems where dispersion forces are very important for the graphite−graphite and water−graphite interaction. For the calculation of energies and gradients, we are using the DFTB implementation by Elstner et al.[32] Geometry optimizations and numerical vibrational frequency calculations were carried out using the optimizer and numerical frequency code of Gaussian 03[42] with Gaussian's external keyword and our own Unix scripts connecting both Gaussian and DFTB programs. QM/MD simulations at the DFTB-D level were done for water, water clusters, and dissociation products of water on the surface of a graphite monolayer model. QM/MD simulations were carried out using the Verlet algorithm using a 0.12 fs time step. The target temperature of 5000 K was maintained using the scaling of velocities approach with 20% overall scaling probability.

For higher level benchmark calculations, we selected the hybrid B3LYP[39] DFT method in combination with Pople's

6-31+G(d) basis set. We have also carried out a limited number of B3LYP/6-311+G(3df,2p) calculations to investigate the effect of larger basis sets, especially on hydrogen, and found no substantial changes in either geometries, energetics, or vibrational frequencies. The B3LYP method is very accurate for standard chemical bonding situations, and we accept the fact that DFT methods in general do not include the description of dispersion forces. After all, charge polarization and electrostatic multipole interactions are most important for water containing systems and are naturally included in DFT. As pointed out by Goddard et al., DFT type calculations with small basis sets are not as susceptible toward the BSSE than MP2 calculations,[43] presumably due to fortuitous error cancellation. For geometry optimizations and vibrational frequency calculations, we have used the B3LYP implementation of Gaussian 03[42] using the default convergence criteria for energies and gradients.

For the calculations of water−graphite interactions and water reactions on graphite surfaces, where extended π-conjugation of the graphite sheet becomes important, we have combined both B3LYP and DFTB-D using the ONIOM integrated method.[37,38]

Results and Discussion

To develop a methodology that reliably leads to the a priori prediction of reaction rate constants for water-induced corrosion processes of graphite at high temperatures without imposing assumptions for reaction pathways, we need to identify high energy reaction mechanisms for systems containing models for bulk graphite with water clusters and water fragments. Traditional force field based water−graphite potentials are incapable of describing bond formation/breaking processes, and pure density functional methods are incapable of describing dispersion forces that are important for the qualitative theoretical treatment of bulk graphite. MP2 or coupled cluster methods that are capable of describing dispersion forces accurately and quantitatively are too expensive for the size of model systems required to describe extended π-conjugation stabilization in graphite correctly. Since we are interested in entire reaction pathways and need to compute long QM/MD simulations as well as vibrational frequencies to characterize TSs, use of the MP2 method is not applicable for our purposes. In the following subsections, we discuss the accuracy of the DFTB-D quantum chemical potential for the description of layer interactions in graphite models; the accuracy of B3LYP/6-31+G(d) and ONIOM(B3LYP/6-31+G(d):DFTB-D) geometries, binding energies, and harmonic vibrational frequencies for systems with water−water and water−graphite interactions; the identification and characterization of dissociative reaction pathways of a water molecule on a single graphite layer by ONIOM; and preliminary high temperature QM/MD DFTB-D trajectories of water clusters and water dissociation products on a graphite surface.

Modeling Bulk Graphite: DFTB-D Optimized Structures and Binding Energies of Graphite Layers. In previous investigations on the electronic structure of graphite, quantum theoretical calculations were carried out typically using periodic boundary conditions.[30,44] However, for the investigation of small molecule interactions with graphite surfaces, cluster calculations were employed as well, with members of the coronene family as model systems for individual graphite layers.[24,45] The electronic and geometrical features of coronene $C_{24}H_{12}$ (C) and polycircumcoronenes have been recently described in the literature.[46] Since the composition of natural graphite is approximately 85% *ABAB*··· (hexagonal) and 15% *ABCABC*··· (rhombohedral),[47] we chose to only include *ABA*-stacked mono- (S_1 or L_1), bi- (S_2 or L_2), and tri- (S_3 or L_3) layers of small $C_{96}H_{24}$ (S) and large $C_{216}H_{36}$ (L) polycircumcoronenes as model systems for hexagonal graphite (see Figure 1). To evaluate the usefulness of the DFTB-D method for describing the π-stacking interaction between graphite layers, we fully optimized the structures of mono- to trilayer S_{1-3} and L_{1-3}. In this work, only pristine (i.e., defect-free) polycircumcoronenes as models for the graphite (0001) surface and bulk graphite were considered. DFTB-D predicts the C−C bond lengths of the central hexagon of both of these graphite models to be 1.425 Å, which is in very good agreement with the experimental C−C bond length of 1.42 Å for bulk graphite.[48] Since the central C−C bond lengths are identical for both S and L models, we conclude that already the S_1 model can be considered converged to bulk graphite in the center of its D_{6h} structure (horizontal bulk effect). The C−C bond lengths begin to alternate toward the polycircumcoronene edges as a consequence of decreasing π-conjugation and reach values between 1.36 Å for the cisoid bonds of the six corners and 1.45 Å for the adjacent 12 transoid bonds. Table 1 shows that the interlayer distances *d* range between 3.18 and 3.20 Å, with shorter distances for $L_{n=2,3}$ due to the increased number of pairwise dispersion terms present in the dispersion function of DFTB-D. Nevertheless, we find that the DFTB-D method reproduces the experimental interlayer distance of bulk graphite satisfactorily well, which is 3.354 Å according to two experiments.[48,49] The experimental interlayer binding energy in the hexagonal graphite has been estimated by different experimental methods and ranges between 0.81 kcal/mol per atom and 1.20 kcal/mol per atom.[48,50,51] Table 1 lists also DFTB-D binding energies with respect to individual graphite layer models, which range between 0.74 kcal/mol per atom and 1.10 kcal/mol per atom (obtained by dividing the total binding energy by the number of carbon atoms) depending on polycircumcoronene size and are in noticeable agreement with the experimental data. It is interesting to note that the interlayer binding energy of the trilayer is larger than 2 times that of the bilayer for both S and L models by a constant amount of about 0.3 kcal/mol per atom, indicating a slight nonlinear increase of the dispersion energy. The third-layer effect is, however, only on the order of 30%, and thus the main contribution of the vertical bulk effect is already included in bilayer model systems. These results indicate that the combined use of polycircumcoronene bilayers as small as S_2 (192 carbon atoms) with the DFTB-D method is appropriate and computationally very feasible for the quantum chemical description of bulk graphite both in two and in three dimensions.

TABLE 1: Binding Energies (BE) and Interlayer Distances (*d*) of DFTB-D Optimized Dimers and Trimers of Small $C_{96}H_{24}$ (S) and Large $C_{216}H_{36}$ (L) Polycircumcoronenes[a]

system	BE (kcal/mol)	calcd. BE/atom	exp. BE/atom	*d* (Å)
S_2	141.5	0.74	0.81[b]	3.200
S_3	294.0	1.02	0.98[c]	3.203
L_2	340.5	0.79	0.81[b]	3.169
L_3	710.2	1.10	0.98[c]	3.177

[a] The experimental interlayer distance (*d*) in graphite is 3.254 Å.[48,49] [b] Ref 50. [c] Ref 48.

Modeling Water−Water and Water−Graphite Interactions: Free $(H_2O)_{n=1-5}$ Clusters and Physisorbed $(H_2O)_{n=1-5}$ Clusters on Graphite. Because of their importance in understanding various phenomena such as solvent effects in biological and chemical systems, the properties (structures, binding energies, vibrational spectra, electronic properties) of small water clusters have been the focus of a large number of experi-

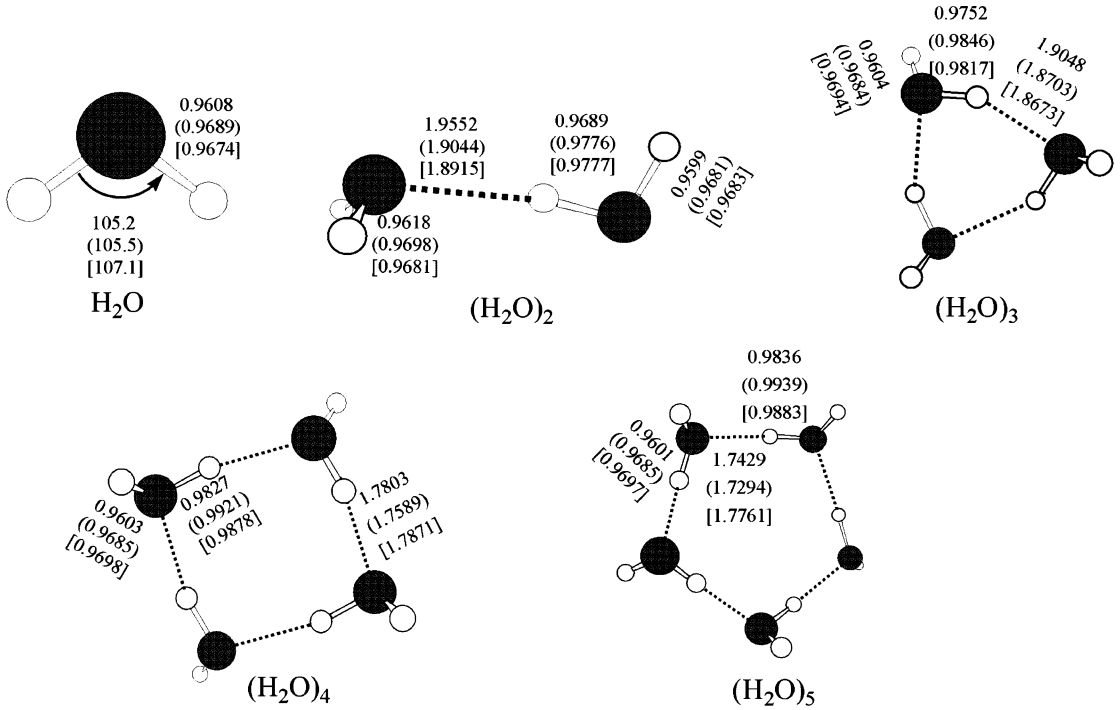

Figure 2. Optimized geometries of water clusters $(H_2O)_{n=1-5}$ calculated by the B3LYP/6-311+G(3df,2p), B3LYP/6-31+G(d) (in parentheses), and DFTB-D (in square brackets) methods. Bond lengths are given in Å.

mental[52−58] and theoretical investigations.[43,59−62] In this subsection, we are presenting B3LYP and DFTB-D structural data for free water clusters $(H_2O)_{n=1-5}$ and compare them with highly accurate MP2 results of Lee et al.[60] Next, structural, energetic, and harmonic vibrational data are presented for various water clusters on monolayers of graphite models C_1 and S_1.

The optimized structures and O−H bond lengths of free cyclic water clusters $(H_2O)_{n=1-5}$ are shown in Figure 2, where we have employed the B3LYP/6-311+G(3df,2p), B3LYP/6-31+G(d), and DFTB-D methods. Intramolecular O−H distances are unproblematic and show only deviations of up to 0.01 Å at all levels of theory. Intermolecular O−H distances, however, are less uniform among different levels, with the large basis set B3LYP calculation showing consistently longer O−H bonds by 0.02−0.05 Å as compared to the B3LYP/6-31+G(d) calculations. This bond length shortening indicates the effect of the larger BSSE for the calculations using a smaller basis set, which typically results in overestimated intermolecular interactions and therefore reduced bond lengths. DFTB-D, on the other hand, predicts intermolecular hydrogen bonds that deviate unsystematically by as much as ±0.06 from B3LYP/6-311+G(3df,2p). Table 2 lists also O−O distances of free $(H_2O)_{n=2-5}$ and includes the MP2/TZ2P++ data by Lee et al.,[60] which is very close to our much more economical B3LYP/6-31+G(d) and even reasonably close to DFTB-D results, when one is willing to accept a ±0.06 Å difference. We would like to stress that particularly the large three-body effect of water clusters is described correctly at all levels of theory employed, namely, the shrinking of the O−O bond by approximately 0.1 Å when comparing the water dimer with the larger water clusters.

This three-body effect is also clearly present when water clusters are physisorbed on a graphite surface, as the water−graphite O−O distances in Table 2 indicate in the three rightmost columns for water clusters on different graphite monolayer sizes and with different methods. The three columns contain O−O distances of $(H_2O)_{n=1-5}$ on C_1 using pure B3LYP/6-31+G(d), on S_1 using ONIOM(B3LYP/6-31+G(d):DFTB-D)

TABLE 2: Geometries of Free $(H_2O)_n$ Clusters and of $(H_2O)_n$ Clusters on Different Models of Graphite Layers[a]

		Free $(H_2O)_n$			$(H_2O)_n$ on Graphite Monolayers		
					C_1	S_1	S_1
n	bond	B3LYP	DFTB-D	MP2	B3LYP	ONIOM	DFTB-D
2	O_1O_2	2.875	2.867	2.904	2.917	2.926	2.876
3	O_1O_2	2.767	2.780	2.793	2.811	2.831	2.795
4	O_1O_2	2.735	2.763	2.738	2.767	2.791	2.763
5	O_1O_2	2.721	2.761	2.724	2.762	2.768	2.767

[a] Only O−O bonds are shown. Bond lengths are given in Å. Only the 6-31+G(d) basis set results for B3LYP are shown, and ONIOM calculations are two-layer ONIOM(B3LYP/6-31+G(d):DFTB-D) with coronene C_1 as the high level model system embedded in the dicircumcoronene S_1 low level real system. MP2 denotes MP2/TZ2P++ calculations of Lee et al.[60]

with C_1 and the water clusters in the high level, and also on S_1 using pure DFTB-D methods from the left to the right, respectively. In the two-layer ONIOM approach, the C_1 high level ONIOM model system is embedded in the S_1 real system, as shown in Figure 3. This choice of ONIOM model allows us to investigate the low level influence of the more extended S_1 π-conjugation on the B3LYP/6-31+G(d) C_1 ONIOM model system properties by comparison with pure B3LYP/6-31+G(d) calculations on C_1−water clusters. In particular, the O−O distance of the water clusters is increased by the presence of the graphite model surface in all three cases. The B3LYP/6-31+G(d) water dimer O−O distance is increased by 0.04 Å due to the presence of C_1, which weakens the intermolecular interaction between the two water molecules due to the added water−graphite attraction. ONIOM takes into account the substituent effect of the larger low level S_1 real system at the DFTB-D level, which leads to a further increase of the O−O bond distance in the B3LYP/6-31+G(d) high level by 0.01−0.02 Å. This indicates that the increased π-conjugation of S_1 in comparison to C_1 slightly influences the water−graphite interaction (horizontal bulk effect). Pure DFTB-D results are less clear concerning the increase of water O−O intermolecular distances due to the physisorption on graphite surfaces, which is on the

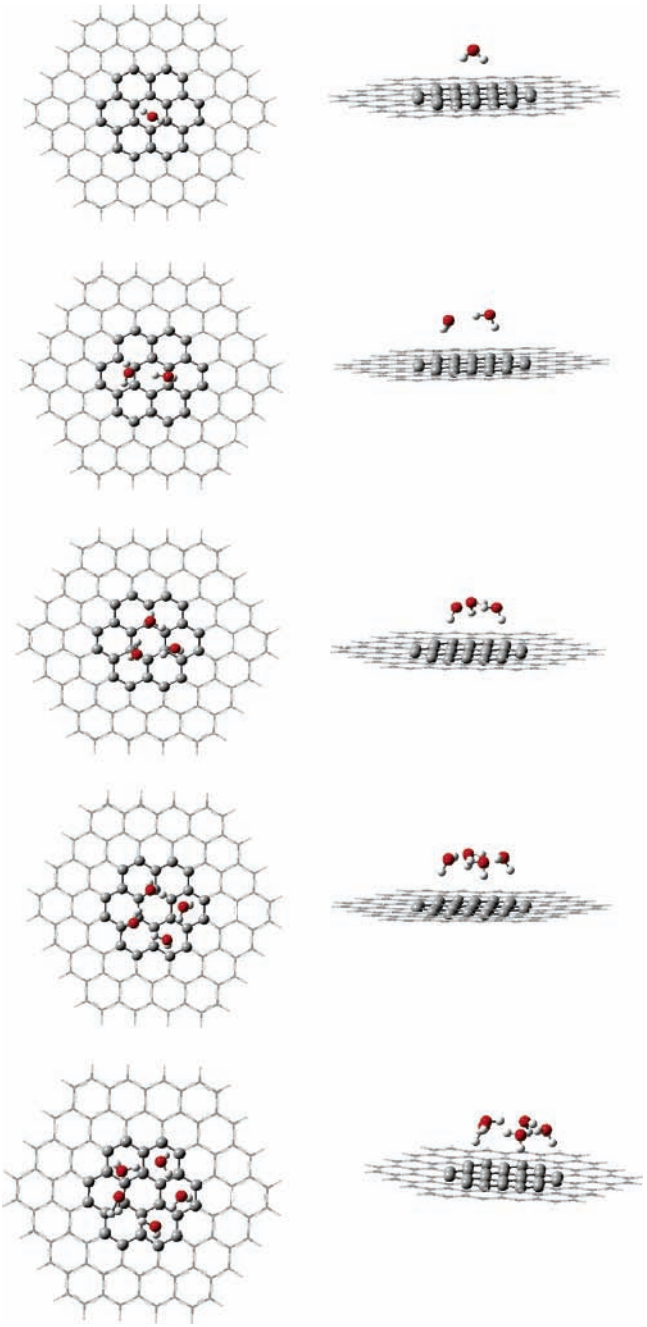

Figure 3. ONIOM(B3LYP/6-31+G(d):DFTB-D) optimized structures of water clusters $(H_2O)_{n=1-5}$ on the surface of a single dicircumcoronene S_1 molecule. Atoms not included in the ONIOM high level model system are represented by a wireframe model. Top view (left) and side view (right).

order of only about 0.01 Å. In summary, from the results of these structural comparisons, we conclude that the characteristic three-body effect of water clusters is preserved in physisorbed water clusters on graphite surfaces and that the ONIOM method reasonably combines the effect of the larger size of the π-conjugated real system at the low level with a higher-level description of the weakened water−water interactions.

Table 3 lists the oxygen−surface distances of physisorbed water clusters on graphite predicted by pure B3LYP, ONIOM, and pure DFTB-D. In general, in our water−graphite monolayer systems, the B3LYP/6-31+G(d) geometry optimizations predict that these distances are mainly in the range between 3.5 and 3.7 Å. This finding is in considerable disagreement with the calculations by Darling et al. who obtained a value of about

TABLE 3: Oxygen−Surface Distances in Å of $(H_2O)_n$ Clusters on Different Models of Graphite Layers[a]

n	O position	B3LYP C_1	ONIOM S_1	DFTB-D S_1	DFTB-D S_2	DFTB-D Δ[b]
1	O_1	3.531	3.397	3.059	3.011	−0.048
2	O_1	3.468	3.454	2.979	2.943	−0.036
	O_2	3.789	3.790	3.333	3.013	−0.320
3	O_1	3.556	3.374	3.191	2.822	−0.369
	O_2	3.676	3.378	3.210	2.932	−0.278
	O_3	3.683	3.417	3.212	3.172	−0.040
4	O_1	3.656	3.385	3.196	2.976	−0.220
	O_2	3.645	3.377	3.195	2.805	−0.390
	O_3	3.651	3.432	3.255	3.035	−0.220
	O_4	3.702	3.469	3.272	3.125	−0.147
5	O_1	3.586	3.392	3.186	2.984	−0.202
	O_2	3.479	3.346	3.164	2.853	−0.311
	O_3	3.450	3.365	3.165	2.876	−0.289
	O_4	3.613	3.429	3.226	3.194	−0.032
	O_5	3.681	3.666	3.232	3.217	−0.015

[a] B3LYP/6-31+G(d) is listed under the column B3LYP, and ONIOM denotes two-layer ONIOM(B3LYP/6-31+G(d):DFTB-D) calculations with S_1 as the real system and C_1 as the high level model. To investigate the vertical bulk graphite effect, water clusters on the S_2 bilayer graphite model were treated at the DFTB-D level of theory. [b] Δ is the difference between oxygen−surface distances of the water−S_1 graphite monomer and the water−S_2 graphite dimer sheets, calculated at the DFTB-D level.

4.0 Å using a nonhybrid DFT method[25] but are in actual good agreement with the more accurate MP2 results by Feller and Jordan, whose oxygen−graphite distance for the water monomer on C_1 is smaller than 3.4 Å. On the other hand, DFTB-D oxygen−surface distances are much shorter with about 3.0−3.2 Å than the B3LYP calculations predict, consistent with stronger DFTB-D water−graphite interactions as observed already in the shorter DFTB-D O−O bonds as compared to B3LYP. The hybrid ONIOM(B3LYP:DFTB-D) method yields oxygen−surface distances that lie between both methods, coincidentally predicting water−surface distances in perfect agreement with the much more expensive MP2.[24]

The oxygen−surface distances are noticeably affected by the presence of an additional *AB* stacked graphite layer, as considerable Δ differences between DFTB-D mono- and bilayer oxygen−surface distances show. We addressed the issue of this vertical bulk effect by placing a second *AB*-stacked S molecule underneath the $S_1-(H_2O)_{n=1-5}$ clusters discussed previously and performing DFTB-D full geometry optimizations. As the shortening of oxygen−surface bond distances Δ by up to almost 0.4 Å shows (see Table 3), the effect of a second graphite layer for the water−surface interaction is indeed not negligible. On the basis of the results of the previous subsection, however, we do not expect that the addition of a third layer would have a dramatic effect on the water−graphite adsorbed structures. For a qualitatively correct treatment of water clusters on graphite in both DFTB-D based QM/MD simulations and ONIOM structure calculations, we therefore conclude that at least a second graphite layer should be included in the model systems.

We would like to address the question of the water monomer on graphite in somewhat more detail, as this has been widely discussed in the theory literature. In the lowest energy conformer of water on benzene, the best calculations show that one hydrogen of the water points toward a carbon atom of the benzene.[28] This conformation was also obtained for the water−coronene and water−circumcoronene structures at the MP2 level of theory[24] and recently for a water−CNT complex using DFT with periodic boundary conditions.[4] However, none of the classical force field methods was able to reproduce the single-legged structure, favoring a two-legged structure where both

TABLE 4: Binding Energies [kcal/mol] of $(H_2O)_{n=1-5}$ Clusters on the Surface of Graphite Layer Models C_1 and S_1/S_2 Calculated at the B3LYP, ONIOM, and DFTB-D, Levels[a]

	$(H_2O)_n$ on C_1		$(H_2O)_n$ on S_1				$(H_2O)_n$ on S_2	
	B3LYP		ONIOM		DFTB-D		DFTB-D	
n	BE_1	BE_2	BE_1	BE_2	BE_1	BE_2	BE_1	BE_2
1	2.1	2.1	1.8	1.8	2.9	2.9	3.2	3.2
2	2.3	8.7	2.3	8.8	4.8	8.2	5.5	8.9
3	2.2	21.4	1.9	21.1	7.1	16.9	7.3	17.1
4	1.1	35.1	1.2	35.2	8.4	26.6	9.6	27.9
5	0.7	45.2	2.6	41.7	10.6	34.4	12.4	36.3

[a] Here, BE_1 and BE_2 stand for the energy of the reactions of graphite$-(H_2O)_n \rightarrow$ graphite $+ (H_2O)_n$ and graphite$-(H_2O)_n \rightarrow$ graphite $+ n(H_2O)$, respectively.

hydrogens are pointing toward the surface, until Pertsin et al. adjusted their inverse power atom−atom potentials to Feller's MP2 structures.[23] This adjustment seemed crucial in describing the wetting behavior of entire water monolayers closer to experimental observations. We found that at both B3LYP and ONIOM(B3LYP:DFTB-D) levels of theory, both minima are practically energetically equivalent with an energy separation of only 0.01 kcal/mol in favor of the two-legged structure. In fact, Zhang et al. report this structure to be the minimum structure for water−coronene at the MP2 level of theory.[41] Apparently, the water monomer can change its orientation very easily on the graphite surface, which is itself not very important but becomes crucial for the development of H-bond networks in larger water clusters on the graphite surface.

Table 4 lists the corresponding binding energies of water clusters $(H_2O)_{n=1-5}$ on mono- and bilayer graphite C and S models. Two different kinds of binding energies are listed: BE_1 stands for the energy of the reaction of graphite$-(H_2O)_n \rightarrow$ graphite $+ (H_2O)_n$, and BE_2 stands for the energy of the reaction of graphite$-(H_2O)_n \rightarrow$ graphite $+ n(H_2O)$. While BE_1 represents a hypothetical interaction between intact water clusters with a graphite surface, BE_2 represents the quantity measurable in desorption experiments when water leaves the surface molecule by molecule. Interestingly, for the ONIOM results of $(H_2O)_{n=1-5}$ on the S_1 monolayer, BE_1 values are about 1.2−2.6 kcal/mol, independent of the number of water molecules. B3LYP/6-31+G(d) binding energies BE_1 for the C_1 graphite model agree with this finding with a difference of only up to 0.3 kcal/mol, which means that the water−graphite interaction is relatively weak and that the water clusters try to maximize H-bond interaction. This is indicated by the linear increase of BE_2, adding between 7.0 and 9.0 kcal/mol per hydrogen bond for both the B3LYP and ONIOM methods, which are again in perfect agreement with each other (difference is less than 0.3 kcal/mol because in both cases water clusters are treated at the B3LYP level of theory). BE_1 and BE_2 of water clusters $(H_2O)_{n=1-5}$ on monomer and dimer S graphite models were also calculated by the DFTB-D method. The energetics is in excellent agreement for the water monomer and dimer, but BE_1 is increasing by about 1.3−2.2 kcal/mol per additional water molecule, which is not the case for the B3LYP and ONIOM calculations discussed previously. Evidently, DFTB-D overestimates the water−graphite interaction as already discussed in the context of structural parameters, and its stronger water−surface interaction is also visible in the lower DFTB-D BE_2 values. Qualitatively, however, DFTB-D paints the same picture as B3LYP or ONIOM: water clusters prefer to maximize the water−water interaction, with very little disturbance by the graphite system. When a second graphite layer is added, BE_1 and BE_2 increase slightly by 0.3−1.9 kcal/mol consistent with the decreased oxygen−surface distances and the notion of stronger water−graphite interaction for bulk graphite. For comparison, the experimental energy of a typical water−water hydrogen bond is about 5 kcal/mol, well-reproduced by BSSE-uncorrected DFT water dimerization energies with 4.9 kcal/mol (B3LYP/6-311+G(3df,2p)) and 6.4 kcal/mol (B3LYP/6-31+G(d)) but somewhat underestimated with 3.4 kcal/mol at the DFTB-D level of theory, respectively.

The harmonic vibrational frequencies of cyclic clusters $(H_2O)_{n=1-6}$ were calculated before using the MP2/aug-cc-pVDZ method[59] and of $(H_2O)_{n=1-10}$ using both the B3LYP/6-311++G(d,p) and the MP2/DZP methods.[60] Recently, Jordan et al. included anharmonicity in their calculation of MP2/aug-cc-pVDZ vibrational frequencies,[61] which can amount to a few hundred wavenumbers for O−H stretch frequencies. We are, however, not so much interested in exactly reproducing experimental vibrational frequencies but in following the frequency shifts associated with physisorption of water clusters on the graphite surface. To the best of our knowledge, no experimental or theoretical vibrational spectra of water clusters on graphite are available, although FTIR spectra were obtained recently for water adsorbed at room temperature on CNTs.[7] Interestingly, Ellison et al. detected peaks corresponding to both physisorbed as well as chemisorbed (C−O stretch and C−H bending vibrations at 1140 and 1360 cm^{-1}, respectively) water, which they explain by assuming water−CNT reactions with chemically more reactive Stone−Wales defects. In Table 5, we present B3LYP/6-31+G(d), DFTB-D and experimental harmonic O−H stretch vibrational frequencies of the free cyclic clusters $(H_2O)_{n=1-5}$, as well as B3LYP/6-31+G(d) data for $(H_2O)_{n=1-3}$ clusters on C_1 and DFTB-D harmonic vibrational frequencies for clusters $(H_2O)_{n=1-5}$ on S_1. The differences between the B3LYP data and the available experimental data for the O−H stretch vibrational frequencies of H_2O and $(H_2O)_2$ are less than ± 17 cm^{-1} but much less accurate in case of the DFTB-D frequencies, which can deviate from experimental frequencies by almost up to 100 wavenumbers (see also ref 63). For free clusters with $n > 2$, we clearly see a distinction between asymmetric ν_a and symmetric ν_s stretch vibrations, with ν_a being much larger by up to 570 cm^{-1} and closer to the water monomer O−H frequencies than ν_s due to hydrogen bonding, as Lee et al. already discussed extensively.[60] Table 5 shows that the ν_a DFTB-D harmonic O−H stretch vibration frequencies of water clusters $(H_2O)_{n=1-5}$ on graphite undergo consistently a 22−35 cm^{-1} red shift and a 6−23 cm^{-1} red shift at the B3LYP/6-31G(d) level of theory. The ν_s harmonic O−H stretch vibration frequencies of water clusters $(H_2O)_{n=1-5}$ on the graphite surface undergo a relatively small shift without consistent direction. The observed red shift of O−H vibrational stretch frequencies is consistent with the changes of O−H bond lengths of the water clusters due to their interaction with the graphite surface.

The data presented previously provide for the first time a sound quantum chemical basis to explain the experimental finding that water can be an effective graphite lubricant while at the same time showing relatively little interaction with graphite surfaces, resulting in steep contact angle of water droplets on graphite surfaces.[22] Clearly, water−graphite interactions are weak, and the potential energy surfaces for the physisorbed water clusters are very flat, yet not repulsive, such that no capillary forces are observed for water intercalated between graphite layers. Temperature programmed desorption data by Kasemo et al.[10] showed that water wets the graphite (0001) surface at least partially, suggesting that water layers

TABLE 5: O−H Stretch Frequencies in cm^{-1} of Free Water Clusters and Water Clusters on the Surface of C_1 and S_1 Model Graphite Monolayers

		Free $(H_2O)_n$			$(H_2O)_n$ on Graphite		Frequency shift	
n	O-H bond type	B3LYP	DFTB-D	exp.	C_1 B3LYP	S_1 DFTB-D	C_1 B3LYP	S_1 DFTB-D
1	ν_a	3861	3982	3943[a]	3850	3953	−11	−29
	ν_s	3737	3711	3832[a]	3737	3685	0	−26
2	ν_a	3856	3977	3899[b]	3842	3949	−14	−28
	ν_a	3825	3905	3881[b]	3819	3882	−6	−22
	ν_s	3739	3708	3797[b]	3732	3681	−7	−27
	ν_s	3625	3572	3718[b]	3624	3577	−1	5
3	ν_a	3827	3890		3811	3855	−16	−35
	ν_a	3826	3882		3803	3854	−23	−28
	ν_a	3822	3879		3800	3853	−22	−26
	ν_s	3549	3527		3539	3536	−10	9
	ν_s	3535	3524		3532	3534	−3	10
	ν_s	3472	3474		3467	3486	−5	12
4	ν_a	3818	3870			3841		−30
	ν_a	3817	3867			3839		−28
	ν_a	3817	3867			3837		−30
	ν_a	3816	3862			3836		−27
	ν_s	3433	3474			3482		8
	ν_s	3393	3457			3466		10
	ν_s	3391	3457			3463		7
	ν_s	3288	3377			3397		20
5	ν_a	3821	3873			3846		−27
	ν_a	3819	3870			3843		−28
	ν_a	3818	3867			3840		−26
	ν_a	3816	3866			3839		−27
	ν_a	3815	3862			3837		−25
	ν_s	3412	3480			3482		2
	ν_s	3398	3471			3480		10
	ν_s	3351	3454			3459		5
	ν_s	3341	3446			3457		11
	ν_s	3249	3380			3399		19

[a] Ref 44. [b] Refs 60 and 61.

were spreading out faster horizontally than vertically. This is consistent with our ONIOM results, where graphite adheres the orientation of the water clusters but allows almost perfect intrawater orientations for maximized H-bond interactions. They also noticed a zero-order kinetic desorption characteristic, indicating that water desorbs not as water clusters but as individual molecules. This picture is consistent with the monotonically increasing BE_2 of both ONIOM and DFTB-D results.

Dissociative Adsorption of Water on Graphite: H_2O−Coronene and H_2O−Dicircumcoronene Reaction System. As a test case for an ONIOM(B3LYP:DFTB-D) exploration of stationary points on the water−graphite reaction system, we found two dissociative adsorption pathways of a water molecule by manual search on a single coronene C_1 and dicircumcoronene S_1 molecule. Figure 4 illustrates these reaction pathways, one connecting all three ortho (P1), meta (P3), and para (P2) products with multiple TSs, the other one connecting reactants and the para-product directly via a single TS_2. Zero-point corrected energetics and imaginary frequencies are given for ONIOM(B3LYP/6-31+G(d):DFTB-D) and DFTB-D using S_1 and for B3LYP/6-31+G(d) and DFTB-D using C_1 graphite monolayers. Compared to corresponding stationary states on the C_1 graphite model, the larger S_1 graphite model shifts TS and product energies down by up to about 8 kcal/mol, indicating that the more extended π-conjugated S_1 system stabilizes sp^3-defects better than the smaller C_1 model. This finding is true for both ONIOM/B3LYP as well as DFTB-D levels of theory and affirms our previous evaluation that a graphite model of size S_1 is required to correctly account for the horizontal bulk graphite effect. Consistent with chemical intuition, the energy order of dissociative water adsorption products is ortho (P1) < para (P2) < meta (P3) at all levels of theory for both graphite models. In a previous ab initio HF/Lanl2dz study on the dissociative adsorption of water on graphite,[29] only two dissociative products for the para and meta positions were found, with the para product being lower in energy than the meta product, consistent with this work. In the following discussion of individual reaction pathways, we will only refer to ONIOM results for model S_1 for the sake of simplicity; other energetics are given in Figure 4, and Cartesian coordinates of all structures at all levels of theory are provided in the Supporting Information. Starting from a weakly bound reactant complex RC1, TS1 leads via a 83.5 kcal/mol barrier to the energetically most favorable ortho addition product P1, which is 65.3 kcal/mol endothermic with respect to the reactants. This ortho product P1 with its very local distortion of the graphite π-conjugation is directly connected with the meta product P3 via a late TS3 with a relative energy of 98.4 kcal/mol. The geometry of the meta product P3 resembles that of an allylic system, with the radical center between C−OH and C−H sp^3 sites. Finally, this product can convert into the para product P2 via a barrier of 6.0 kcal/mol for TS4. As to the direct pathway to P2, we find that a TS2 with 92.1 kcal/mol relative energy exists, connecting a prepositioned water molecule with hydrogen atoms pointing in 1,4-positions of the closest graphite hexagon in structure RC2 with the asymmetric dissociation product P2, which is endothermic with respect to reactants by 70.5 kcal/mol energy. All transition states have been confirmed by vibrational mode analysis and possess only one imaginary frequency, which can differ on the order of several hundred wavenumbers between DFTB-D, B3LYP, and ONIOM(B3LYP:DFTB-D). However, qualitatively, DFTB-D predicts the same TSs as B3LYP at a small fraction of the computational cost and can therefore be ef-

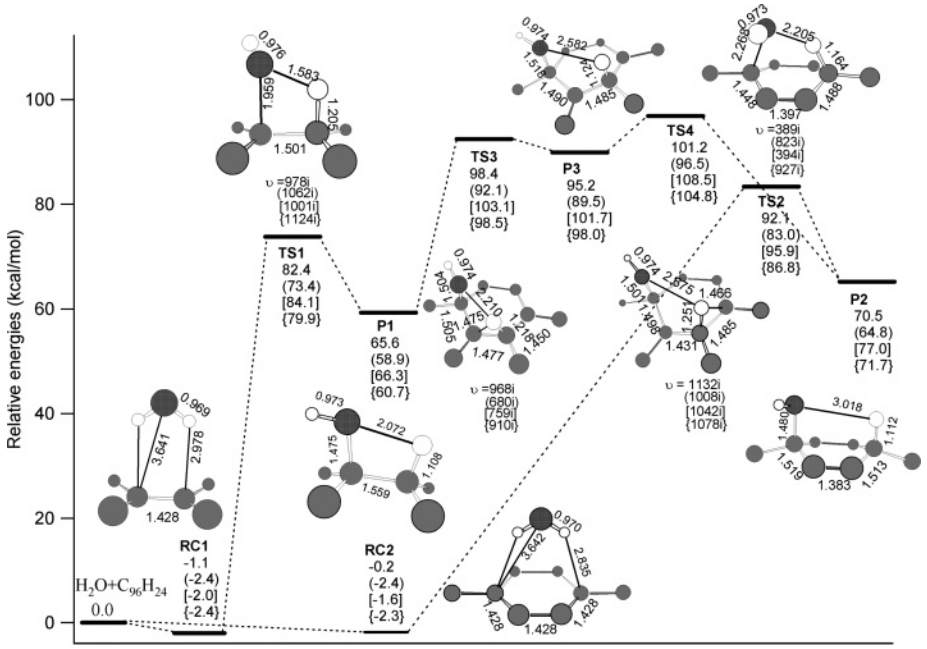

Figure 4. Schematic reaction pathways, zero-point corrected energetics, and optimized stationary structures of reactants, products, and transition states of two water dissociative reactions on C_1 and S_1 graphite model systems. Plain numbers denote ONIOM(B3LYP/6-31+G(d):DFTB-D) results, numbers in parentheses denote DFTB-D results using the S_1 graphite model, and numbers in square and curly brackets denote B3LYP/6-31+G(d) and DFTB-D results using the C_1 graphite model, respectively.

ficiently used in the search for TSs, before more expensive ONIOM calculations are employed for more accurate characterization. IRC calculations verifying the reaction pathways were only carried out at the DFTB-D level of theory for the C_1 model, as IRC calculations are computationally extremely demanding.

The rate constants of the one-step H_2O dissociative adsorption reactions via RC1 to P1 and RC2 to P2 on S_1 have been predicted by the ChemRate program,[64] based on the energetics and vibrational frequencies obtained by the ONIOM(B3LYP/6-31+G(d):DFTB-D) method. According to ChemRate, the predicted rate constants for the two processes

$$H_2O + S_1 \rightarrow P1$$

$$H_2O + S_1 \rightarrow P2$$

in the temperature range from 1000 to 5000 K can be represented, respectively, by the expressions in units of cm^3/s

$$k_1 = 1.5 \times 10^{-27} \times \exp(-46\,300/T)$$

$$k_2 = 1.7 \times 10^{-28} \times \exp(-51\,100/T)$$

The rate constants for the dissociative adsorption processes (k_i) are defined by

$$d[X]_{surf}/dt = k_i(\theta/A_s)[X]_g$$

which has the unit of a flux, molecule/cm^2/s. In the rate equation, θ represents the fraction of available surface sites, A_s is the surface area, and $[X]_g$ is the gas-phase concentration of H_2O in molecules/cm^3. The previous result means that on account of the very high barriers and low rate constants for the dissociative adsorption processes, the dissociative reactions of H_2O on a defect-free graphite surface can only occur at extremely high temperatures. This finding is contrasted by the observations by Ellison et al., who claim to see a large amount of chemisorbed water on CNTs at room temperature.[7] Their finding needs to be viewed in the light that side-wall curvature and Stone−Wales, vacancy, oxidation, and other defects make CNTs more reactive than pristine graphite. In future studies, we will also include model systems for graphite defects.

QM/MD Simulations of Water, Water Clusters, and Water Dissociative Adsorption Products on Graphite Models. Preliminary QM/MD simulations of water, water clusters, and water dissociative adsorption products P2, P3, and P1 on the surface of the S_1 graphite monolayer were carried out using the DFTB-D quantum chemical potential at a temperature of 5000 K, to simulate graphite corrosion due to fuel combustion with water as a major exhaust product. Simulation times did not exceed 40 fs because chemistry happens rapidly at such high temperatures. In cases where water was only physisorbed on the graphite surface, water molecules moved quickly away from the surface. The larger water clusters $(H_2O)_{3-5}$ display the same dynamic behavior as the water dimer at $T = 5000$ K, namely, dissociation with a highly distorted graphite sheet and individual water molecules as products. Naturally, at this high temperature, the binding energy of a few kcal/mol for the water−graphite complex is not strong enough to keep water molecules sticking to the graphite surface, nor to themselves. In general, in our QM/MD simulations at 5000 K, we do notice chemical transformations of the graphite slab, in particular at its borders, where polyacetylene chain formation is observed similar to the polyyne chain formation visible in DFTB QM/MD simulations of pure carbon at high temperatures.[34−36]

Dynamics simulations starting with the dissociative adsorption para product P2 at 5000 K lead to rapid recombination of the dissociated H and OH fragments due to their proximity to form a water molecule and consequently move away from the graphite slab, and the S_1 dicircumcoronene is observed to completely heal the sp^3 defects. This process is achieved in less than 5 fs at 5000 K.

Dynamics simulations starting with the least stable dissociative adsorption product P3 at times show its transformation from meta to the ortho adsorption product, before recombining and water detachment. The relative energy of P3 is 31.8 kcal/mol higher than P1 and 26.6 kcal/mol higher than P2. Therefore, it

is understandable that the dynamics shows the P3 transformation to the most stable product P1 in a time frame under 10 fs.

Finally, dynamics simulations starting with the energetically most stable dissociative adsorption product P1 show the rapid recombination of the dissociated H and OH and detachment of water similar as was the case for P2. In this trajectory, the S_1 graphite model undergoes the greatest transformations at its borders to yield a free-floating polyacetylene chain, but they can be observed for trajectories of all three different reaction products.

These preliminary QM/MD simulations indicate that graphite surfaces are indeed chemically very inert and fast self-healing. In addition, as we have pointed out earlier, graphite bilayer models will be required to include the vertical bulk graphite effect at least qualitatively. QM/MD simulations along these lines are currently underway in our laboratory.

Summary

We investigated in detail the interaction of water clusters $(H_2O)_{n=1-5}$ on the graphite (0001) surface using a variety of quantum chemical methods, namely, B3LYP with the 6-31+G-(d) and larger basis sets, dispersion augmented self-consistent-charge DFTB (DFTB-D), and the integrated MO:MO ONIOM-(B3LYP/6-31+G(d):DFTB-D) method. Mono- (C_1, S_1, or L_1), bi- (S_2 or L_2), and trilayers (S_3 or L_3) of coronene $C_{24}H_{12}$ (C), dicircumcoronene $C_{96}H_{24}$ (S), and tetracircumcoronene $C_{216}H_{36}$ (L) were used to model bulk graphite. We laid out a methodology to a priori compute reaction rate constants for water-induced graphite corrosion processes at high temperatures, using a three stage strategy: (1) isokinetic DFTB-D QM/MD simulations were carried out at high temperatures to probe bias-free reaction pathways for water and its dissocation products on dimers of graphite layer models; (2) identification and characterization of stationary points along these pathways using the ONIOM-(B3LYP/6-31+G(d):DFTB-D) level of theory with C_1 and the water molecules and/or fragments in the ONIOM high level model system; and (3) calculation of reaction rate constants based on the characterized TSs. In this paper, we have successfully demonstrated the suitability of each of the quantum chemical methods employed in stages 1 and 2 by comparing our results with available experimental or higher level theoretical data and investigated the water cluster interactions and water reactions with models for bulk graphite. In particular, we have shown that: (a) DFTB-D reproduces the experimental bulk graphite C−C bond length in the centers of both S and L models, and it also reproduces experimental interlayer distances and binding energies of bulk graphite reasonably well. *AB* stacked bi-layers of S with 192 carbon atoms are sufficiently large to mimic 100% of horizontal and 70% of vertical bulk effects. (b) B3LYP/6-31+G(d) reproduces much more expensive counterpoise corrected MP2 and DFT optimized geometries and harmonic vibrational frequencies of free water clusters to a very good degree. (c) ONIOM(B3LYP/6-31+G(d):DFTB-D) with C_1 and water in the ONIOM high level and S_2 as the low level real graphite model system capture water cluster−graphite interactions at the level of B3LYP, with DFTB-D reasonably including the vertical as well as horizontal graphite bulk effect in the low level. ONIOM also reproduces extensive MP2 oxygen−surface distances at a fraction of the computational cost. (d) Geometries, vibrational spectra, as well as energetics are consistent with the experimental observation of weakly interacting water droplets that can freely move over graphite surfaces. Water monomers can freely rotate on the surfaces but are forced into a more rigid single-legged conformation by building a water cluster H-bond network. (e) π-Conjugation effects are successfully included in the ONIOM(B3LYP/6-31+G(d):DFTB-D) investigations of reaction pathways, with reactants, intermediates, TSs, and products effectively described with B3LYP/6-31+G(d) accuracy. (f) High temperature QM/MD simulations using DFTB-D are computationally feasible and provide consistent results with energetics obtained at the much more expensive ONIOM(B3LYP:DFTB-D) level of theory.

In future investigations, we will include the second graphite layer model in QM/MD simulations and ONIOM identifications and characterizations of stationary points, investigate the reactions of multiple water molecules with the S_2 graphite model, and investigate the effect of intercalated water between graphite layers as well as defective graphite layers, which should exhibit a greater reactivity.

Acknowledgment. We thank Prof. Marcus Elstner, University of Paderborn, Germany, for making the DFTB code available to us. Prof. Eric Borguet at Temple University is acknowledged for very helpful discussions on TPD data. We gratefully acknowledge financial support from the Office of Naval Research under a MURI grant. M.C.L. acknowledges support from the National Science Council of Taiwan for a Distinguished Visiting Professorship at the National Chiao Tung University in Hsinchu, Taiwan. SX thanks the Cherry L. Emerson Center of Emory University for a Visiting Fellowship, and the authors acknowledge the Emerson Center for the use of its resources.

Note Added in Proof: After this paper was submitted for publication, a related MP2 and DFTB-D study on water cluster physisorption on graphite was published as Lin, C. S.; Zhang, R. Q.; Lee, S. T.; Elstner, M.; Frauenheim, Th.; Wan, L. J. *J. Phys. Chem. B* **2005**, *109* (29), 14183−14188. Their findings concerning physisorption energies and cluster structures are very similar to ours.

Supporting Information Available: Figure S1 shows select molecular dynamics snapshot structures for the QM/MD simulations of water clusters and water dissociation products on the surface of the $\mathbf{S}_1$ graphite model using the DFTB-D method. Table S1 lists O−H stretch frequencies in [cm^{-1}] of free water clusters calculated at the B3LYP/ 6-311+G(3df,2p) level of theory. Table S2 lists levels of theory, graphite models, and imaginary frequencies for all structures of the reaction pathway study of subsection 3.3 as well as total energies for respective levels of theory. Table S3 lists corresponding Cartesian coordinates.

References and Notes

(1) Marti, J.; Gordillo, M. C. *J. Chem. Phys.* **2001**, *114*, 10486.
(2) Marti, J.; Gordillo, M. C. *Phys. Rev. B* **2001**, *63*, 165430.
(3) Marti, J.; Gordillo, M. C. *Phys. Rev. B* **2001**, *64*, 021504.
(4) Pati, R.; Zhang, Y.; Nayak, S. K.; Ajayan, P. M. *Appl. Phys. Lett.* **2002**, *81*, 2638.
(5) Bekyarova, E.; Hanzawa, Y.; Kaneko, K.; Silvestre-Albero, J.; Sepulveda-Escribano, A.; Rodriguez-Reinoso, F.; Kasuya, D.; Yudasaka, M.; Iijima, S. *Chem. Phys. Lett.* **2002**, *366*, 463−468.
(6) Gordillo, M. C.; Marti, J. *Phys. Rev. B* **2003**, *67*, 205425.
(7) Ellison, M. D.; Good, A. P.; Kinnaman, C. S.; Padgett, N. E. *J. Phys. Chem. B* **2005**, *109*, 10640.
(8) Lancaster, J. K. *Tribology Int.* **1990**, *23*, 371.
(9) Zaidi, H.; Paulmier, D.; Lepage, J. *Appl. Surf. Sci.* **1990**, *44*, 221.
(10) Chakarov, D. V.; Oesterlund, L.; Kasemo, B. *Vacuum* **1995**, *46*, 1109.
(11) Vartapetyan, R. S.; Voloshchuk, A. M.; Isirikyan, A. A.; Polyakov, N. S.; Tarasevich, Y. I. *Colloids Surf., A* **1995**, *101*, 227.
(12) Foley, N. J.; Thomas, K. M.; Forshaw, P. L.; Stanton, D.; Norman, P. R. *Langmuir* **1997**, *13*, 2083.

(13) Harding, A. W.; Foley, N. J.; Norman, P. R.; Francis, D. C.; Thomas, K. M. *Langmuir* **1998**, *14*, 3858.
(14) Salame, I. I.; Bagreev, A.; Bandosz, T. J. *J. Phys. Chem. B* **1999**, *103*, 3877.
(15) Lopez-Ramon, M. V.; Stoeckli, F.; Moreno-Castilla, C.; Carrasco-Marπn, F. *Carbon* **2000**, *38*, 825−829.
(16) Phillips, J.; Kelly, D.; Radovic, L.; Xie, F. *J. Phys. Chem. B* **2000**, *104*, 8170.
(17) Maddox, M.; Ulberg, D.; Gubbins, K. E. *Fluid Phase Equilib.* **1995**, *104*, 145.
(18) Muller, E. A.; Rull, L. F.; Vega, L. F.; Gubbins, K. E. *J. Phys. Chem.* **1996**, *100*, 1189.
(19) McCallum, C. L.; Bandosz, T. J.; McGrother, S. C.; Müller, E. A.; Gubbins, K. E. *Langmuir* **1999**, *15*, 533.
(20) Tomsic, A.; Markovic, N.; Pettersson, J. B. C. *Chem. Phys. Lett.* **2000**, *329*, 200.
(21) Tomsic, A.; Andersson, P. U.; Markovic, N.; Pettersson, J. B. C. *J. Chem. Phys.* **2003**, *119*, 4916.
(22) Werder, T.; Walther, J. H.; Jaffe, R. L.; Halicioglu, T.; Koumoutsakos, P. *J. Phys. Chem. B* **2003**, *107*, 1345.
(23) Pertsin, A.; Grunze, M. *J. Phys. Chem. B* **2004**, *108*, 1357.
(24) Feller, D.; Jordan, K. D. *J. Phys. Chem. A* **2000**, *104*, 9971.
(25) Cabrera, P.; Holloway, S.; Kolasinski, K. W.; Darling, G. R. *Surf. Sci.* **2002**, *532*−*535*, 166.
(26) Ludwig, R.; Appelhagen, A. *Angew. Chem., Int. Ed.* **2005**, *44*, 811.
(27) Boys, S. F.; Bernardi, F. *Mol. Phys.* **1970**, *19*, 553.
(28) Feller, D. *J. Phys. Chem. A* **1999**, *103*, 7558.
(29) Zhanpeisov, N. U.; Harada, M.; Anpo, M. *J. Mol. Struct. (THEOCHEM)* **2000**, *529*, 135.
(30) Porezag, D.; Frauenheim, T.; Koehler, T.; Seifert, G.; Kaschner, R. *Phys. Rev. B* **1995**, *51*, 12947.
(31) Seifert, G.; Porezag, D.; Frauenheim, T. *Int. J. Quantum Chem.* **1996**, *58*, 185.
(32) Elstner, M.; Porezag, D.; Jungnickel, G.; Frauenheim, T.; Suhai, S.; Seifert, G. *Phys. Rev. B* **1998**, *58*, 7260.
(33) Kumar, A.; Elstner, M.; Suhai, S. *Int. J. Quantum. Chem.* **2003**, *95*, 44.
(34) Irle, S.; Zheng, G.; Elstner, M.; Morokuma, K. *Nano Lett.* **2003**, *3*, 1657.
(35) Irle, S.; Zheng, G.; Elstner, M.; Morokuma, K. *High Temperature Quantum Chemical Molecular Dynamics Simulations of Carbon Nanostructure Self-Assembly Processes; Theory and Applications of Computational Chemistry: The First 40 Years*; Seoul, Korea, 2004.
(36) Zheng, G.; Irle, S.; Morokuma, K. *J. Chem. Phys.* **2005**, *122*, 014708.
(37) Maseras, F.; Morokuma, K. *J. Comput. Chem.* **1995**, *16*, 1170.
(38) Matsubara, T.; Maseras, F.; Koga, N.; Morokuma, K. *J. Phys. Chem.* **1996**, *100*, 2573.
(39) Becke, A. D. *J. Chem. Phys.* **1993**, *98*, 5648.
(40) Frauenheim, T.; Seifert, G.; Elstner, M.; Hajnal, Z.; Jungnickel, G.; Porezag, D.; Suhai, S.; Scholz, R. *Phys. Status Solidi B* **2000**, *217*, 41.
(41) Lin, C. S.; Zhang, R. Q.; Lee, S. T.; Elstner, M.; Frauenheim, T.; Wan, L. J. *J. Phys. Chem. B* **2005**, *109*, 14183.
(42) Frisch, M. J.; Trucks, G. W.; Schlegel, H. B.; Scuseria, G. E.; Robb, M. A.; Cheeseman, J. R.; Montgomery, J. A., Jr.; Vreven, T.; Kudin, K. N.; Burant, J. C.; Iyengar, S. S.; Millam, J. M.; Tomasi, J.; Barone, V.; Mennucci, B.; Cossi, M.; Scalmani, G.; Rega, N.; Petersson, G. A.; Ehara, M.; Toyota, K.; Hada, M.; Fukuda, R.; Hasegawa, J.; Ishida, M.; Nakajima, T.; Kitao, O.; Nakai, H.; Honda, Y.; Nakatsuji, H.; Li, X.; Knox, J. E.; Hratchian, H. P.; Cross, J. B.; Adamo, C.; Jaramillo, J. J.; Cammi, R.; Pomelli, C.; Gomperts, R.; Stratmann, R. E.; Ochterski, J.; Ayala, P. Y.; Morokuma, K.; Salvador, P.; Dannenberg, J. J.; Zakrzewski, V. G.; Dapprich, S.; Daniels, A. D.; Strain, M. C.; Farkas, O.; Malick, D. K.; Rabuck, A. D.; Raghavachari, K.; Foresman, J. B.; Ortiz, J. V.; Cui, Q.; Baboul, A. G.; Clifford, S.; Cioslowski, J.; Stefanov, B. B.; Liu, G.; Liashenko, A.; Piskorz, P.; Komaromi, I.; Martin, R. L.; Fox, D. J.; Keith, T.; Al-Laham, M. A.; Peng, C. Y.; Nanayakkara, A.; Challacombe, M.; Gill, P. M. W.; Johnson, B.; Chen, W.; Wong, M. W.; Gonzalez, C.; Pople, J. A. *Gaussian 03*, Revision C.1; Pittsburgh, PA, 2004.
(43) Su, J. T.; Xu, X.; Goddard, W. A., III *J. Phys. Chem. A* **2004**, *108*, 10518.
(44) Yin, M. T.; Cohen, M. L. *Phys. Rev. B* **1984**, *29*, 6996.
(45) Bauschlicher, C. W., Jr.; Ricca, A. *Phys. Rev. B* **2004**, *70*, 115409/1.
(46) Dias, J. R. *THEOCHEM* **2002**, *581*, 59.
(47) Palser, A. H. R. *Phys. Chem. Chem. Phys.* **1999**, *1*, 4459.
(48) Girifalco, L. A.; Lad, R. A. *J. Chem. Phys.* **1956**, *25*, 693.
(49) Kinoshita, K. *Carbon*−*Electrochemical and Physicochemical Properties*; John Wiley & Sons: New York, 1988; p 23.
(50) Benedict, L. X.; Chopra, N. G.; Cohen, M. L.; Zettl, A.; Louie, S. G.; Crespi, V. H. *Chem. Phys. Lett.* **1998**, *286*, 490.
(51) Zacharia, R.; Ulbricht, H.; Hertel, T. *Phys. Rev. B* **2004**, *69*, 155406.
(52) Pugliano, N.; Saykally, R. J. *Science* **1992**, *257*, 1937.
(53) Liu, K.; Brown, M. G.; Carter, C.; Saykally, R. J.; Gregory, J. K.; Clary, D. C. *Nature* **1996**, *381*, 501.
(54) Gregory, J. K.; Clary, D. C.; Liu, K.; Brown, M. G.; Saykally, R. J. *Science* **1997**, *275*, 814.
(55) Fellers, R. S.; Leforestier, C.; Braly, L. B.; Brown, M. G.; Saykally, R. J. *Science* **1999**, *284*, 945.
(56) Nauta, K.; Miller, R. E. *Science* **2000**, *287*, 293.
(57) Fajardo, M. E.; Tam, S. *Science* **2001**, *115*, 6807.
(58) Ludwig, R. *Angew. Chem., Int. Ed.* **2001**, *40*, 1808.
(59) Xantheas, S. S.; Dunning, T. H., Jr. *J. Chem. Phys.* **1993**, *99*, 8774.
(60) Lee, H. M.; Suh, S. B.; Lee, J. Y.; Tarakeshwar, P.; Kim, K. S. *J. Chem. Phys.* **2000**, *112*, 9759.
(61) Diri, K.; Myshakin, E. M.; Jordan, K. D. *J. Phys. Chem. A* **2005**, *109*, 4005.
(62) Lenz, A.; Ojamäe, L. *Phys. Chem. Chem. Phys.* **2005**, *2005*, 1905.
(63) Witek, H.; Irle, S.; Morokuma, K. *J. Chem. Phys.* **2004**, *121*, 5163.
(64) Mokrushin, W.; Bedanov, V.; Tsang, W.; Zachariah, M.; Knyazev, V. *ChemRate, Version 1.20*; National Institute of Standards and Technology: Gaithersburg, MD, 2003.